Soluble Flt-1 Gene Transfer Ameliorates Neointima Formation After Wire Injury in flt-1 Tyrosine Kinase–Deficient Mice

Jun-ichiro Koga, Tetsuya Matoba, Kensuke Egashira, Mitsuki Kubo, Miho Miyagawa, Eiko Iwata, Katsuo Sueishi, Masabumi Shibuya, Kenji Sunagawa

Objective—We have demonstrated that vascular endothelial growth factor (VEGF) expression is upregulated in injured vascular wall, and blockade of VEGF inhibited monocyte infiltration and neointima formation in several animal models. In the present study, we aimed to clarify relative role of two VEGF receptors, flt-1 versus flk-1/KDR, in neointima formation after injury using flt-1 tyrosine kinase-deficient (Flt-1 $TK^{-/-}$) mice and soluble Flt-1(sFlt-1) gene transfer.

Methods and Results—Neointima formation was comparable between wild-type and Flt-1 $TK^{-/-}$ mice 28 days after intraluminal wire injury in femoral arteries. By contrast, neointima formation was significantly suppressed by sFlt-1 gene transfer into Flt-1 $TK^{-/-}$ mice that blocks VEGF action on flk-1 (intima/media ratio: 2.8 ± 0.4 versus 1.4 ± 0.4, $P<0.05$). The inhibition of neointima formation was preceded by significant reduction of monocyte chemoattractant protein (MCP-1) expression in vascular smooth muscle cells (VSMCs) and monocyte infiltration 7 days after injury. Gene transfer of sFlt-1 or treatment of flk-1–specific antibody significantly inhibited VEGF-induced MCP-1 expression determined by RT-PCR in cultured aortic tissue and VSMCs. MCP-1–induced chemotaxis was equivalent between wild-type and Flt-1 $TK^{-/-}$ mice.

Conclusions—These results suggest that endogenous VEGF accelerates neointima formation through flk-1 by regulating MCP-1 expression in VSMCs and macrophage-mediated inflammation in injured vascular wall in murine model of wire injury. (***Arterioscler Thromb Vasc Biol.* 2009;29:458-464.**)

Key Words: restenosis ■ inflammation ■ smooth muscle cells ■ angiogenesis

Vascular endothelial growth factor (VEGF) is one of the most potent angiogenic and vascular permeability factors playing essential roles in neonatal and postnatal vascular formation. VEGF has gathered growing attention because of its possible contribution to cardiovascular pathophysiology including therapeutic angiogenesis, endothelial regeneration, and inflammation in the vascular wall. VEGF expression is upregulated in human coronary arterial wall after stent implantation, suggesting its role in reendothelialization, perivascular angiogenesis, and neointima formation leading to clinical restenosis.[1] VEGF induction is reproduced in various animal vascular injury models including wire or cuff injury in mice, and balloon injury in rats and rabbits, porcine coronary stent model.[2–4] From these prior studies that supplement or inhibit VEGF pathway in animal models, two conflicting mechanisms have been demonstrated in which VEGF may contribute to neointima formation. One is that VEGF inhibits neointima formation by promoting reendothelialization and inhibiting vascular smooth muscle cell (VSMC) proliferation.[5] The other is that VEGF accelerates neointima formation by promoting inflammation[2,4] and adventitial angiogenesis in the vascular wall.[2,3,6]

In this controversy, clinical studies have been carried out to examine the effect of VEGF gene delivery after percutaneous coronary angioplasty without significant reduction in restenosis.[7–9] Thus, it is crucial to understand the mechanisms underlying differential effects of VEGF during neointima formation to optimize vasculoprotective effects and minimize adverse effects of endogenous VEGF that may depend on receptor, cell type, and the mode of vascular injury including species studied. We have demonstrated that flt-1 (VEGF receptor 1) is upregulated during neointima formation after vascular injury, especially in the neointima, media, and adventitia, and flk-1/KDR (VEGF receptor 2) in the neointima and media, and that blockade of VEGF by soluble Flt-1 (sFlt-1) gene transfer inhibited monocyte infiltration and neointima formation in several animal models.[2,4] However, contribution of each VEGF receptor was not fully clarified in

Received December 2, 2007; revision accepted January 7, 2009.

From the Department of Cardiovascular Medicine (J.K., T.M., K.E., M.K., M.M., E.I., K. Sunagawa) and the Division of Pathophysiological and Experimental Pathology (K. Sueishi), Graduate School of Medical Sciences, Kyushu University, Fukuoka, Japan; and the Department of Molecular Oncology (M.S.), Graduate School of Medicine and Dentistry, Tokyo Medical and Dental University, Tokyo, Japan.

Correspondence to Kensuke Egashira, MD, PhD, Department of Cardiovascular Medicine, Graduate School of Medical Sciences, Kyushu University, 3-1-1, Maidashi, Higashi-ku, Fukuoka 812-8582, Japan. E-mail egashira@cardiol.med.kyushu-u.ac.jp

Arterioscler Thromb Vasc Biol **is available at http://atvb.ahajournals.org** **DOI: 10.1161/ATVBAHA.109.183772**

previous studies including ours, because sFlt-1 as well as other VEGF traps sequesters VEGF from its receptors nonspecifically.[2,10] It is reported that flk-1/KDR mainly mediates endothelial cell proliferation during angiogenesis,[11] so that flk-1 may promote reendothelialization and suppress neointima formation after injury. By contrast, flt-1 is reported to regulate nitric oxide production in endothelial cells,[12] and to regulate monocyte chemotaxis that may promote inflammation and influence neointima formation.[13] Therefore, the present study aimed to determine the relative role of each VEGF receptor, flt-1 versus flk-1, in neointima formation after vascular injury, using flt-1 tyrosine kinase-deficient (Flt-1 $TK^{-/-}$) mice[14] in the presence or absence of sFlt-1 gene transfer[2,15] in wire injury model.

Methods

Experimental Animals

All study protocols were reviewed and approved by the Committee on the Ethics of Animal Experiments in Kyushu University Graduate School of Medical Sciences. To examine the role of flt-1, we used Flt-1 $TK^{-/-}$ mice on C57Bl/6J background because flt-1 deficiency is known to be embryonic lethal.[14] Age-matched C57Bl/6J mice (CLEA Japan, Tokyo, Japan) were used as wild-type (WT) control. All mice were fed with normal diet and water at libitum.

Expression Vector

The 3.3-kb mouse *sFLT-1* gene, originally cloned from mouse lung cDNA library, was subcloned into the *Bam*H I (5′) and *Not* I (3′) sites of the eukaryotic expression vector cDNA3 plasmid (Invitrogen, Carlsbad, Calif).[2,16]

Femoral Arterial Wire Injury

To examine the role of flt-1 in neointima formation, femoral arterial wire injury was performed in male 12- to 20-week-old WT or Flt-1 $TK^{-/-}$ mice. After exposure of left femoral artery, straight spring wire (0.38 mm in diameter, COOK) was inserted into femoral artery from the muscular branch. The wire was placed for 1 minute to denude and dilate the artery. After removal of wire, branch artery was ligated and restoration of blood flow was verified by pulsation of peripheral arteries.[2,17] Twenty-eight days after injury, femoral artery was excised after injection of 10% buffered formalin and evaluated histopathologically. Heart rate and systolic blood pressure were measured by tail cuff method before sacrifice.

Soluble Flt-1 Gene Transfer

To examine the role of flk-1, sFlt-1 gene transfer was performed in Flt-1 $TK^{-/-}$ mice as described elsewhere.[2,4,15] Briefly, plasmid vector encoding sFlt-1 cDNA (100 μg) was injected in the gastrocnemial muscle followed by electroporation to facilitate gene transfer. sFlt-1 gene transfer was performed once every 2 weeks from 14 days before until 28 days after injury, based on the data that serum sFlt-1 concentration was elevated over 28 days after single injection of sFlt-1 plasmid with the peak at 14 day after injection (serum sFlt-1concentration at baseline and 3, 14, and 28 days after injection was 222±24, 396±59,* 970±55,* and 477±54* pg/mL, *$P<0.05$ versus baseline).

Histopathology and Immunohistochemistry

For histopathologic and immunohistochemical analysis, serial paraffin sections of the femoral artery were prepared. Briefly, femoral artery was excised after perfusion of 10% buffered formalin and fixed overnight in formalin. After fixation, the tissue was embedded in paraffin and cross sections (6 μm thick) were stained with Masson trichrome or elastica van Gieson stains. Neointima area was defined as the area surrounded by internal elastic lamina except lumen area. Extent of neointima formation was evaluated by the areal ratio of intima to media (I/M ratio) and neointima area. Other sections were subjected to immunostaining using rat anti-mouse macrophage monoclonal antibodies (Mac-3; BD Pharmingen), goat antimouse monocyte chemoattractant protein-1 (MCP-1) antibodies (Santa Cruz Biotechnology Inc). Proliferating cells were evaluated by the immunostaining with antiproliferating cell nuclear antigen (PCNA) antibody (DAKO). Alpha-smooth muscle actin (α-SMA, DAKO) and CD31 antibody (Santa Cruz) were also used as smooth muscle and endothelium marker. The respective nonimmune IgGs were used as negative controls. After incubation with biotinylated goat antirat IgG (Santa Cruz Biotechnology Inc) or rabbit anti-goat IgG (Nichirei), the sections were incubated with diaminobenzidine (DAB). The sections were then counterstained with Mayer hematoxylin. Analysis was performed using a microscope with a computerized, digital image analysis system and Scion Image Software (Scion Corporation). Fluorescent immunostaining was performed with secondary antibodies which are labeled by AlexaFluor 488 or 555 (Invitrogen).

Ex Vivo Culture of Mouse Aorta

Male 12- to 20-week-old WT Flt-1 $TK^{-/-}$ and sFlt-1 plasmid-injected Flt-1 $TK^{-/-}$ mice were used in this experiment. In the first experiment, sFlt-1 plasmid was injected 7 days before excision of aorta. Aorta was excised from ascending aorta to the bifurcation of iliac arteries and incubated with Dulbecco modified Eagle medium (DMEM) containing 1% fetal bovine serum (FBS). After overnight starvation, aorta was incubated with 50 ng/mL VEGF for 3 hours. Then, mRNA was extracted and quantitative real-time RT-PCR was performed by ABI PRISM 7000 Sequence Detection System (Applied Biosystems). MCP-1 and GAPDH primer, which is mixed with probes as TaqMan Gene Expression Assays, were commercially available and purchased from Applied Biosystems. The second experiment was performed using WT mice and blocking antibody of flt-1(R&D Systems Inc) and flk-1 (R&D Systems Inc). After overnight incubation with these antibodies, mRNA was collected in a similar fashion.

VEGF-Induced MCP-1 Expression in VSMCs

Mouse aortic VSMCs (P53LMACO1)[18] was purchased from Health Science Research Resource Banks and cultured in DMEM containing 10% FBS and phorbol-12myristate-13acetate (PMA, 100 nmol/L). VSMCs were used after 9 passages in the experiment. VSMCs were starved overnight and incubated with blocking antibody for flt-1 (10 μg/mL, R&D Systems) or flk-1 (1 μg/mL, R&D Systems). MCP-1 gene expression was analyzed by real-time PCR after 4-hour stimulation with 200 ng/mL human VEGF.

Peritoneal Macrophage Chemotaxis

Peritoneal fluid containing macrophage was harvested 4 days after intraperitoneal injection of thioglycolate. Macrophage migration was measured in 96-well chemotaxis chambers (Neuro Probe Inc). MCP-1 or VEGF in RPMI 1640 was added to the lower wells and the isolated macrophages (1×10^7 cells per mL) were placed in the upper wells. The concentration of MCP-1 and VEGF was 5, 15, and 50 ng/mL. After incubation for 90 minutes at 37°C, the upper surface of the membrane was washed with PBS and migrated cells on the lower surface were counted after staining with trypan blue. The number of cells per field was counted. All assays were performed in triplicate.

Statistics

All data are reported as the mean±SE. Statistical analysis of differences was performed by Student *t* test and 1-way ANOVA with Bonferroni post test. Statistical analysis of chemotaxis assay was performed by 2-way ANOVA with Bonferroni post test. Probability values less than 0.05 were considered to be statistically significant.

Results

Distinct Role of flt-1 and flk-1 in Neointima Formation After Wire Injury

To examine the role of flt-1 in neointima formation, we examined the degree of neointima formation after wire injury

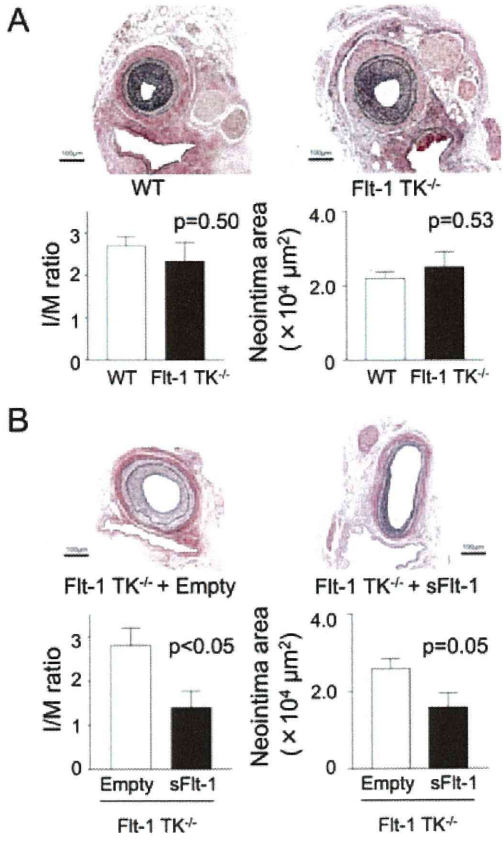

Figure 1. Distinct effects of flt-1 TK deficiency and sFlt-1 gene transfer on neointima formation. Neointima formation was comparable in wild-type (WT, n=7) and Flt-1 $TK^{-/-}$ mice (n=8) 28 days after wire injury (A). Neointima formation was significantly inhibited in Flt-1 $TK^{-/-}$ mice transfected with sFlt-1 plasmid (n=6) compared with empty plasmid (Empty, n=6; B). Scale bar indicates 100 μm.

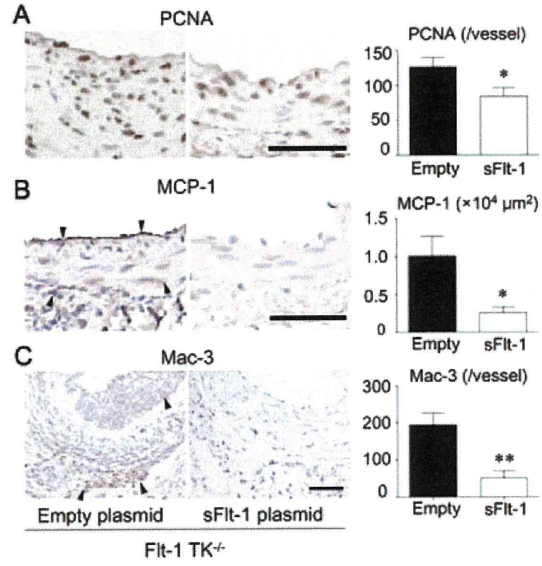

Figure 2. Gene transfer of sFlt-1 in Flt-1 $TK^{-/-}$ mice decreased PCNA-positive cells in the neointima (A), MCP-1 expression in the endothelial layer and medial cells (B), and Mac-3–positive monocytes/macrophages in the neointima and the adventitia (C) 7 days after injury (n=5 to 6 for each group). Scale bar indicate 50 μm. *$P<0.05$, **$P<0.01$ vs empty plasmid group. Arrowheads (▼) indicates stained cells.

in femoral arteries of Flt-1 $TK^{-/-}$ mice. Flt-1 $TK^{-/-}$ mice lack intracellular tyrosine kinase domain of flt-1 and thus downstream signaling.[14] Histological analysis revealed that there was no significant difference in I/M ratio and neointimal area 28 days after wire injury between WT and Flt-1 $TK^{-/-}$ mice (Figure 1A), suggesting that the role of flt-1 is minor in neointima formation in this model. Deficiency of flt-1 tyrosine kinase unaffected heart rate (673±11 versus 662±19 bpm) or blood pressure (110±3 versus 104±3 mm Hg) in mice, also unaffected macrophage infiltration evaluated as mac-3 staining, perivascular fibrosis and vessel diameter (data not shown).

To examine the role of flk-1, sFlt-1 gene transfer was performed into Flt-1 $TK^{-/-}$ mice. The sFlt-1 sequesters VEGF from both VEGF receptors and thus we could evaluate the role of flk-1 when applied to Flt-1 $TK^{-/-}$ mice. The sFlt-1 gene transfer markedly inhibited neointima formation with significant reduction of I/M ratio compared with control empty plasmid in Flt-1 $TK^{-/-}$ mice (Figure 1B). The sFlt-1 gene transfer did not affect heart rate (662±19 versus 660±11 bpm) and blood pressure (95±5 versus 107±4 mm Hg) in Flt-1 $TK^{-/-}$ mice.

sFlt-1 Gene Transfer Suppressed Proliferation, Monocyte Infiltration, and MCP-1 Expression in Flt-1 $TK^{-/-}$ Mice

We have repeatedly shown the importance of MCP-1 and monocyte-mediated inflammation in the vascular wall during vascular remodeling in various vascular disease models.[19–22] Thus, we analyzed the effect of sFlt-1 gene transfer on proliferation of vascular wall cells, MCP-1 expression, and monocyte/macrophage infiltration at an early stage of neointima formation. Histology at 7 days after injury showed a decrease in PCNA-positive cells in the neointima of Flt-1 $TK^{-/-}$ mice transfected with sFlt-1 gene that underpins reduction in neointima formation (Figure 2A). Prominent MCP-1 induction was found in the intimal and the medial cells in Flt-1 $TK^{-/-}$ mice, which was markedly suppressed by sFlt-1 gene transfer (Figure 2B). Infiltration of Mac-3–positive monocytes was found in the media and adventitia, which was suppressed by sFlt-1 gene transfer as well (Figure 2C). These results suggest that endogenous VEGF upregulates MCP-1 and macrophage recruitment via flk-1 in Flt-1 $TK^{-/-}$ mice during neointima formation after wire injury.

Distinct Role of flt-1 and flk-1 in VEGF-Mediated MCP-1 Induction

To elucidate detailed mechanisms of VEGF-mediated MCP-1 induction in injured arteries, we first performed double immunostaining of MCP-1 and α-SMA 3 days after injury when the endothelium has not regenerated yet. We found equivalent MCP-1 induction in the medial VSMCs in WT and Flt-1 $TK^{-/-}$ mice. In contrast, sFlt-1 gene transfer into Flt-1 $TK^{-/-}$ mice remarkably inhibited MCP-1 induction (Figure 3A). These results suggest that (1) wire injury induces MCP-1 expression primarily in the VSMCs and (2) flk-1, but not

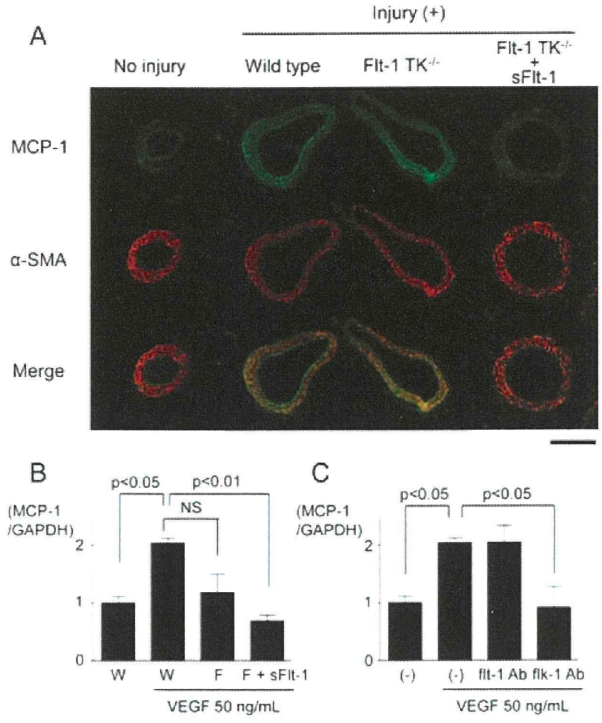

Figure 3. Blockade of flk-1 suppressed MCP-1 induction in VSMCs in vivo and ex vivo. Immunostaining of MCP-1 and α-SMA revealed that MCP-1 is induced in the medial VSMCs 3 days after injury (A). Scale indicates 200 μm. VEGF-induced MCP-1 expression in cultured aortas was inhibited by sFlt-1 gene transfer (B, n=3 each) and anti–flk-1 antibody (C, n=3 each). W: wild type mice, F: Flt-1 $TK^{-/-}$ mice.

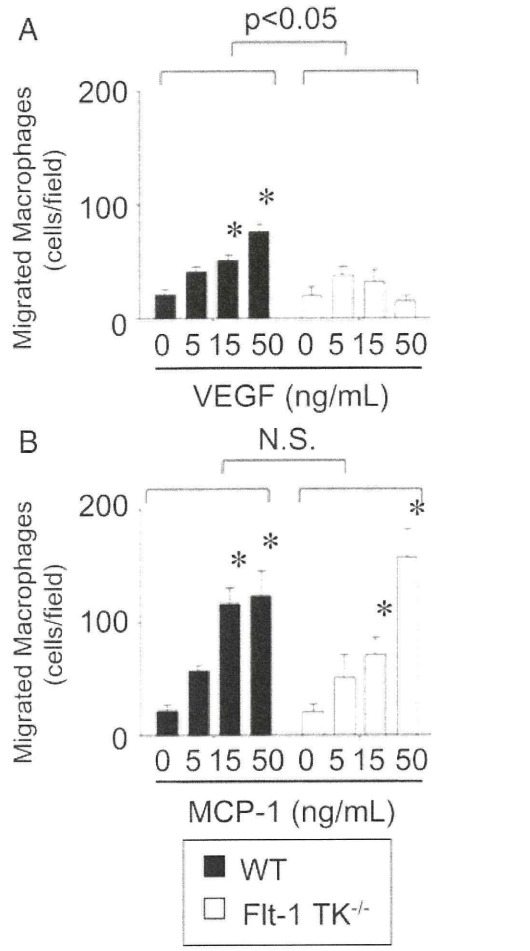

Figure 4. Flt-1 TK deficiency blunted VEGF-induced chemotaxis of macrophages. Chemotaxis of peritoneal macrophage to VEGF or MCP-1 was examined in Boyden chamber experiments. VEGF induced significant chemotaxis in WT mice, which was blunted in Flt-1 $TK^{-/-}$ mice (A). MCP-1 induced prominent and equivalent chemotaxis in WT and Flt-1 $TK^{-/-}$ mice (B). n=6 to 7 for each group. *$P<0.05$ vs control.

flt-1, mediates MCP-1 induction in the VSMCs immediately after vascular injury. Next, we examined the role of each VEGF receptor in MCP-1 induction in ex vivo culture model. Mouse aorta was harvested from WT, Flt-1 $TK^{-/-}$, and sFlt-1 plasmid-administrated Flt-1 $TK^{-/-}$ mice. The aortas were stimulated with VEGF (50 ng/mL) after 24-hour starvation, and induction of MCP-1 was quantified by real-time PCR. Real-time PCR showed that VEGF-induced expression of MCP-1, which is partially but not significantly inhibited by Flt-1 TK deletion and is completely inhibited by sFlt-1 gene transfer, suggesting that VEGF-induced MCP-1 mRNA transcription is primarily mediated by flk-1 (Figure 3B). Blockade of each VEGF receptor by neutralizing antibodies showed that anti–flt-1 antibody had no effect; by contrast, anti–flk-1 antibody completely inhibited VEGF-induced MCP-1 expression (Figure 3C). Finally we examined the effect of each VEGF receptor blockade on VEGF-induced MCP-1 expression in mouse aortic VSMCs. Blocking antibody of flt-1 did not inhibit VEGF-induced MCP-1 expression. In contrast, blocking antibody of flk-1 significantly inhibited VEGF-induced MCP-1 expression (supplemental Figure I, please see http://atvb.ahajournals.org). These results suggest that VEGF induces MCP-1 expression by flk-1–mediated mechanisms in mouse VSMCs. We also examined whether blockade of VEGF influences PDGF signaling that may mediate MCP-1 induction in injured arterial wall.[23] In vitro study using cultured VSMCs revealed that blockade of VEGF by sFlt-1 gene transfer or sFlt-1 protein does not inhibit PDGF-induced phosphorylation of PDGF receptors, suggesting that blockade of flk-1 inhibit MCP-1 induction via PDGF-independent mechanisms (supplemental Figure II).

Macrophage Chemotaxis in WT and Flt-1 $TK^{-/-}$ Mice

It is reported that human monocytes exclusively express flt-1 and that VEGF induces chemotaxis by flt-1–mediated mechanism.[13] We performed Boyden chamber experiment to examine macrophage chemotactic function in response to VEGF or MCP-1 in WT and Flt-1 $TK^{-/-}$ mice. VEGF induced significant chemotaxis of peritoneal macrophage from WT mice, which was abolished by Flt-1 TK deficiency (Figure 4A), suggesting that flt-1 essentially mediates VEGF-induced chemotaxis. By contrast, MCP-1 caused more prominent chemotaxis in WT and Flt-1 $TK^{-/-}$ mice equivalently (Figure 4B). These results suggest that MCP-1–induced chemotaxis was preserved in Flt-1 $TK^{-/-}$ mice, and MCP-1 is a primary mediator of flk-1–dependent macrophage recruitment in injured vascular wall even in the Flt-1 TK deficiency.

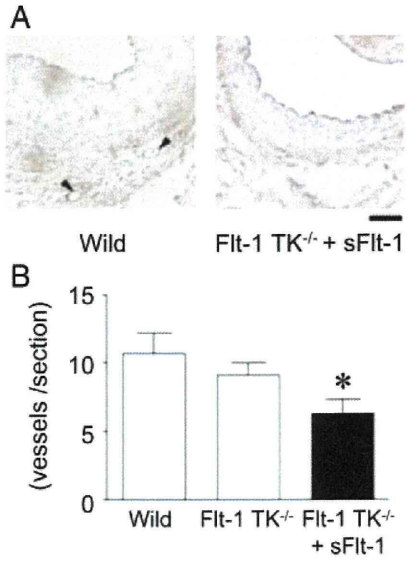

Figure 5. Adventitial angiogenesis was evaluated by CD31 immunostaining 28 days after wire injury (A). sFlt-1 gene transfer into Flt-1 $TK^{-/-}$ mice inhibited adventitial angiogenesis compared with wild mice (B). n=7 for each group. *$P<0.05$ versus wild type.

Effect of sFlt-1 Gene Transfer on Adventitial Angiogenesis

Adventitial angiogenesis was evaluated by counting CD31-positive endothelial cells in the adventitia of injured femoral arteries. Adventitial angiogenesis was equivalent in WT and Flt-1 $TK^{-/-}$ mice, however, was significantly decreased in Flt-1 $TK^{-/-}$ mice after sFlt-1 gene transfer compared with WT mice (Figure 5).

Discussion

In this study, we aimed to clarify the relative importance of 2 VEGF receptors, flt-1 and flk-1/KDR in neointima formation after intraluminal wire injury. Major findings were: (1) Flt-1 TK deficiency unaffected neointima formation, (2) sFlt-1 gene transfer into Flt-1 $TK^{-/-}$ mice remarkably suppressed neointima formation, and (3) VEGF induced MCP-1 expression in VSMCs which was blocked by flk-1–specific antibody. The inhibition of neointima formation by flk-1 blockade was preceded by significant reduction of MCP-1 expression in the medial VSMCs 3 days after injury, and monocyte infiltration, VSMC proliferation, and perivascular neovascularization 7 days after injury. These in vivo results suggest that flk-1 plays a primary role in the development of neointima by regulating macrophage-mediated inflammation in this model.

Inflammation in the vascular wall, mainly mediated by monocyte and macrophage, is a hallmark of vascular remodeling after injury as evident in our previous studies using cuff injury in mice and balloon injury in rats, rabbits, and monkeys, in which MCP-1 blockade effectively suppresses vascular inflammation and remodeling.[24–26] It is reported that VEGF induces MCP-1 expression in endothelial cells[27]; in turn, MCP-1 induces VEGF in VSMCs.[28] Macrophage-mediated inflammation activates VSMC migration and proliferation by cytokines, or by redox-dependent signaling.[29,30]

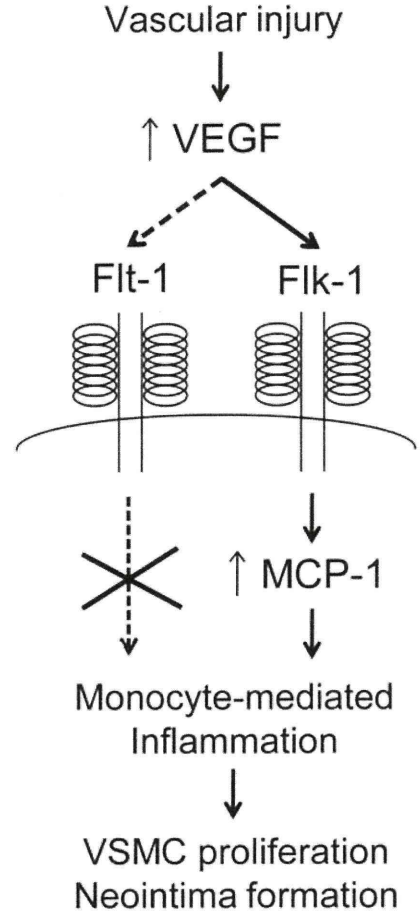

Figure 6. Flk-1 accelerates neointima formation after vascular injury. VEGF is upregulated in vascular wall cells after wire injury. VEGF activates flk-1 to cause MCP-1 induction and monocyte recruitment to the injured vascular wall. Monocyte/macrophage-mediated inflammation results in VSMC proliferation and neointima formation. Flt-1–mediated monocyte chemotaxis is minor to cause neointima formation in vivo, as indicated by dotted lines.

Although flk-1 is expressed mainly in endothelial cells, VSMCs also express flk-1,[31] and the present study revealed a new mechanism that flk-1 mediates MCP-1 expression in VSMCs and monocyte recruitment after injury. This VEGF/MCP-1–positive feedback and downstream signaling is considered to be a major underlying mechanism in neointima formation after injury, as shown in our previous studies using sFlt-1 and MCP-1 mutant[19,24–26] (Figure 6).

It has been reported that VEGF induces direct macrophage chemotaxis by flt-1–mediated mechanisms, whereas flk-1 is not expressed on monocytes/macrophages.[13] Indeed, Flt-1 TK deficiency abrogated VEGF-induced chemotaxis in peritoneal macrophages in the present study; however, Flt-1 TK deficiency had no effect on macrophage infiltration into injured arterial wall and neointima formation in in vivo setting. In the present study, blockade of flk-1 inhibited MCP-1 expression in the medial VSMCs and abrogated monocyte accumulation in the vascular wall after injury. Thus, we considered that MCP-1, which is regulated by VEGF/flk-1 pathway, mainly mediates macrophage chemo-

taxis rather than VEGF/flt-1 expressed on monocyte itself. This mechanism well explains the in vivo effect of flk-1 blockade on monocyte accumulation after injury.

In the present study, sFlt-1 gene transfer also inhibited adventitial angiogenesis after injury. Inhibition of adventitial angiogenesis may be another mechanism by which flk-1 blockade inhibits neointima formation, because a positive correlation was observed between adventitial blood vessel formation and neointima formation in various injury model including rabbit collar placement model.[32]

The role of VEGF in neointima formation may be different depending on the mode of injury or the species studied. For example, Isner et al[33] reported that local delivery of VEGF accelerates reendothelialization and attenuates intimal hyperplasia in balloon-injured rat carotid artery. Hutter et al[5] reported in mouse wire injury model that intravenous injection of VEGF adenovirus promoted endothelial repair and inhibited neointima formation. By contrast, Khurana et al[32] reported that adenovirus-mediated VEGF gene transfer exacerbates adventitial neovascularization and neointima formation in rabbit periadventitial collar replacement model, which was abrogated by administration of sFlt-1. Thus, there remain controversies in the role of VEGF gene transfer per se in neointima formation in previous studies. In the present study, we administered sFlt-1 plasmid intramuscularly, and sFlt-1, which was detected in the serum, blocked VEGF signaling at the site of vascular injury. In our previous study, we have reported that reendothelialization is complete 14 days after wire injury in mice irrespective of VEGF blockade by sFlt-1 gene transfer.[2] Thus, it is suggested that on complete reendothelialization, excess VEGF may accelerate neointima formation by promoting monocyte-mediated inflammation through flk-1–dependent MCP-1 expression in the injured vascular wall at least in the murine wire injury model studied. In this situation, Flk-1–specific VEGF blockade may be another potential approach to control vascular inflammation and subsequent remodeling after injury.

In conclusion, the present study demonstrated that soluble sFlt-1 gene transfer ameliorates neointima formation after wire injury in flt-1 tyrosine kinase–deficient mice by inhibiting MCP-1 expression in the medial VSMCs and resulting monocyte-mediated inflammation. The present findings suggest that endogenous VEGF accelerates neointima formation after injury through flk-1–dependent mechanisms, and provide new insights into complex VEGF-mediated signaling in vascular remodeling.

Sources of Funding

This study was supported by Grants-in-Aid for Scientific Research (19390216, 19650134) from the Ministry of Education, Science, and Culture, Tokyo, Japan and by Health Science Research Grants (Research on Translational Research and Nano-medicine) from the Ministry of Health Labor and Welfare, Tokyo, Japan.

Disclosures

None.

References

1. Brasen JH, Kivela A, Roser K, Rissanen TT, Niemi M, Luft FC, Donath K, Yla-Herttuala S. Angiogenesis, vascular endothelial growth factor and platelet-derived growth factor-BB expression, iron deposition, and oxidation-specific epitopes in stented human coronary arteries. *Arterioscler Thromb Vasc Biol.* 2001;21:1720–1726.
2. Ohtani K, Egashira K, Hiasa K, Zhao Q, Kitamoto S, Ishibashi M, Usui M, Inoue S, Yonemitsu Y, Sueishi K, Sata M, Shibuya M, Sunagawa K. Blockade of vascular endothelial growth factor suppresses experimental restenosis after intraluminal injury by inhibiting recruitment of monocyte lineage cells. *Circulation.* 2004;110:2444–2452.
3. Shibata M, Suzuki H, Nakatani M, Koba S, Geshi E, Katagiri T, Takeyama Y. The involvement of vascular endothelial growth factor and flt-1 in the process of neointimal proliferation in pig coronary arteries following stent implantation. *Histochem Cell Biol.* 2001;116:471–481.
4. Zhao Q, Egashira K, Hiasa K, Ishibashi M, Inoue S, Ohtani K, Tan C, Shibuya M, Takeshita A, Sunagawa K. Essential role of vascular endothelial growth factor and Flt-1 signals in neointimal formation after periadventitial injury. *Arterioscler Thromb Vasc Biol.* 2004;24:2284–2289.
5. Hutter R, Carrick FE, Valdiviezo C, Wolinsky C, Rudge JS, Wiegand SJ, Fuster V, Badimon JJ, Sauter BV. Vascular endothelial growth factor regulates reendothelialization and neointima formation in a mouse model of arterial injury. *Circulation.* 2004;110:2430–2435.
6. Bhardwaj S, Roy H, Heikura T, Yla-Herttuala S. VEGF-A, VEGF-D and VEGF-D(DeltaNDeltaC) induced intimal hyperplasia in carotid arteries. *Eur J Clin Invest.* 2005:669–676.
7. Hedman M, Hartikainen J, Syvanne M, Stjernvall J, Hedman A, Kivela A, Vanninen E, Mussalo H, Kauppila E, Simula S, Narvanen O, Rantala A, Peuhkurinen K, Nieminen MS, Laakso M, Yla-Herttuala S. Safety and feasibility of catheter-based local intracoronary vascular endothelial growth factor gene transfer in the prevention of postangioplasty and in-stent restenosis and in the treatment of chronic myocardial ischemia: phase II results of the Kuopio Angiogenesis Trial (KAT). *Circulation.* 2003;107:2677–2683.
8. Laitinen M, Hartikainen J, Hiltunen MO, Eranen J, Kiviniemi M, Narvanen O, Makinen K, Manninen H, Syvanne M, Martin JF, Laakso M, Yla-Herttuala S. Catheter-mediated vascular endothelial growth factor gene transfer to human coronary arteries after angioplasty. *Hum Gene Ther.* 2000;11:263–270.
9. Shiojima I, Walsh K. The role of vascular endothelial growth factor in restenosis: the controversy continues. *Circulation.* 2004;110:2283–2286.
10. Kendall RL, Wang G, Thomas KA. Identification of a natural soluble form of the vascular endothelial growth factor receptor, FLT-1, and its heterodimerization with KDR. *Biochem Biophys Res Commun.* 1996;226:324–328.
11. Millauer B, Wizigmann-Voos S, Schnurch H, Martinez R, Moller NP, Risau W, Ullrich A. High affinity VEGF binding and developmental expression suggest Flk-1 as a major regulator of vasculogenesis and angiogenesis. *Cell.* 1993;72:835–846.
12. Bussolati B, Dunk C, Grohman M, Kontos CD, Mason J, Ahmed A. Vascular endothelial growth factor receptor-1 modulates vascular endothelial growth factor-mediated angiogenesis via nitric oxide. *Am J Pathol.* 2001;159:993–1008.
13. Barleon B, Sozzani S, Zhou D, Weich HA, Mantovani A, Marme D. Migration of human monocytes in response to vascular endothelial growth factor (VEGF) is mediated via the VEGF receptor flt-1. *Blood.* 1996;87:3336–3343.
14. Hiratsuka S, Minowa O, Kuno J, Noda T, Shibuya M. Flt-1 lacking the tyrosine kinase domain is sufficient for normal development and angiogenesis in mice. *Proc Natl Acad Sci U S A.* 1998;95:9349–9354.
15. Zhao Q, Ishibashi M, Hiasa K, Tan C, Takeshita A, Egashira K. Essential role of vascular endothelial growth factor in angiotensin II-induced vascular inflammation and remodeling. *Hypertension.* 2004;44:264–270.
16. Kondo K, Hiratsuka S, Subbalakshmi E, Matsushime H, Shibuya M. Genomic organization of the flt-1 gene encoding for vascular endothelial growth factor (VEGF) receptor-1 suggests an intimate evolutionary relationship between the 7-Ig and the 5-Ig tyrosine kinase receptors. *Gene.* 1998;208:297–305.
17. Sata M, Maejima Y, Adachi F, Fukino K, Saiura A, Sugiura S, Aoyagi T, Imai Y, Kurihara H, Kimura K, Omata M, Makuuchi M, Hirata Y, Nagai R. A mouse model of vascular injury that induces rapid onset of medial cell apoptosis followed by reproducible neointimal hyperplasia. *J Mol Cell Cardiol.* 2000;32:2097–2104.
18. Masuda T, Ohmi K, Yamaguchi H, Hasegawa K, Sugiyama T, Matsuda Y, Iino M, Nonomura Y. Growing and differentiating characterization of aortic smooth muscle cell line, p53LMAC01 obtained from p53 knock out mice. *Mol Cell Biochem.* 1999;190:99–104.

19. Egashira K. Molecular mechanisms mediating inflammation in vascular disease: special reference to monocyte chemoattractant protein-1. *Hypertension*. 2003;41:834–841.
20. Egashira K, Nakano K, Ohtani K, Funakoshi K, Zhao G, Ihara Y, Koga J, Kimura S, Tominaga R, Sunagawa K. Local delivery of anti-monocyte chemoattractant protein-1 by gene-eluting stents attenuates in-stent stenosis in rabbits and monkeys. *Arterioscler Thromb Vasc Biol*. 2007;27: 2563–2568.
21. Inoue S, Egashira K, Ni W, Kitamoto S, Usui M, Otani K, Ishibashi M, Hiasa K, Nishida K, Takeshita A. Anti-monocyte chemoattractant protein-1 gene therapy limits progression and destabilization of established atherosclerosis in apolipoprotein E-knockout mice. *Circulation*. 2002;106:2700–2706.
22. Nakano K, Egashira K, Ohtani K, Zhao G, Funakoshi K, Ihara Y, Sunagawa K. Catheter-based adenovirus-mediated anti-monocyte chemoattractant gene therapy attenuates in-stent neointima formation in cynomolgus monkeys. *Atherosclerosis*. 2007;194:309–316.
23. Marumo T, Schini-Kerth VB, Fisslthaler B, Busse R. Platelet-derived growth factor-stimulated superoxide anion production modulates activation of transcription factor NF-kappaB and expression of monocyte chemoattractant protein 1 in human aortic smooth muscle cells. *Circulation*. 1997;96:2361–2367.
24. Egashira K, Zhao Q, Kataoka C, Ohtani K, Usui M, Charo IF, Nishida K, Inoue S, Katoh M, Ichiki T, Takeshita A. Importance of monocyte chemoattractant protein-1 pathway in neointimal hyperplasia after periarterial injury in mice and monkeys. *Circ Res*. 2002;90:1167–1172.
25. Ohtani K, Usui M, Nakano K, Kohjimoto Y, Kitajima S, Hirouchi Y, Li XH, Kitamoto S, Takeshita A, Egashira K. Antimonocyte chemoattractant protein-1 gene therapy reduces experimental in-stent restenosis in hypercholesterolemic rabbits and monkeys. *Gene Ther*. 2004;11: 1273–1282.
26. Usui M, Egashira K, Ohtani K, Kataoka C, Ishibashi M, Hiasa K, Katoh M, Zhao Q, Kitamoto S, Takeshita A. Anti-monocyte chemoattractant protein-1 gene therapy inhibits restenotic changes (neointimal hyperplasia) after balloon injury in rats and monkeys. *Faseb J*. 2002;16: 1838–1840.
27. Yamada M, Kim S, Egashira K, Takeya M, Ikeda T, Mimura O, Iwao H. Molecular mechanism and role of endothelial monocyte chemoattractant protein-1 induction by vascular endothelial growth factor. *Arterioscler Thromb Vasc Biol*. 2003;23:1996–2001.
28. Parenti A, Bellik L, Brogelli L, Filippi S, Ledda F. Endogenous VEGF-A is responsible for mitogenic effects of MCP-1 on vascular smooth muscle cells. *Am J Physiol Heart Circ Physiol*. 2004;286:H1978–H1984.
29. Griendling KK, FitzGerald GA. Oxidative stress and cardiovascular injury: Part I: basic mechanisms and in vivo monitoring of ROS. *Circulation*. 2003;108:1912–1916.
30. Viedt C, Vogel J, Athanasiou T, Shen W, Orth SR, Kubler W, Kreuzer J. Monocyte chemoattractant protein-1 induces proliferation and interleukin-6 production in human smooth muscle cells by differential activation of nuclear factor-kappaB and activator protein-1. *Arterioscler Thromb Vasc Biol*. 2002;22:914–920.
31. Ishida A, Murray J, Saito Y, Kanthou C, Benzakour O, Shibuya M, Wijelath ES. Expression of vascular endothelial growth factor receptors in smooth muscle cells. *J Cell Physiol*. 2001;188:359–368.
32. Khurana R, Zhuang Z, Bhardwaj S, Murakami M, De Muinck E, Yla-Herttuala S, Ferrara N, Martin JF, Zachary I, Simons M. Angiogenesis-dependent and independent phases of intimal hyperplasia. *Circulation*. 2004;110:2436–2443.
33. Asahara T, Bauters C, Pastore C, Kearney M, Rossow S, Bunting S, Ferrara N, Symes JF, Isner JM. Local delivery of vascular endothelial growth factor accelerates reendothelialization and attenuates intimal hyperplasia in balloon-injured rat carotid artery. *Circulation*. 1995;91: 2793–2801.

Supplemental Figure I

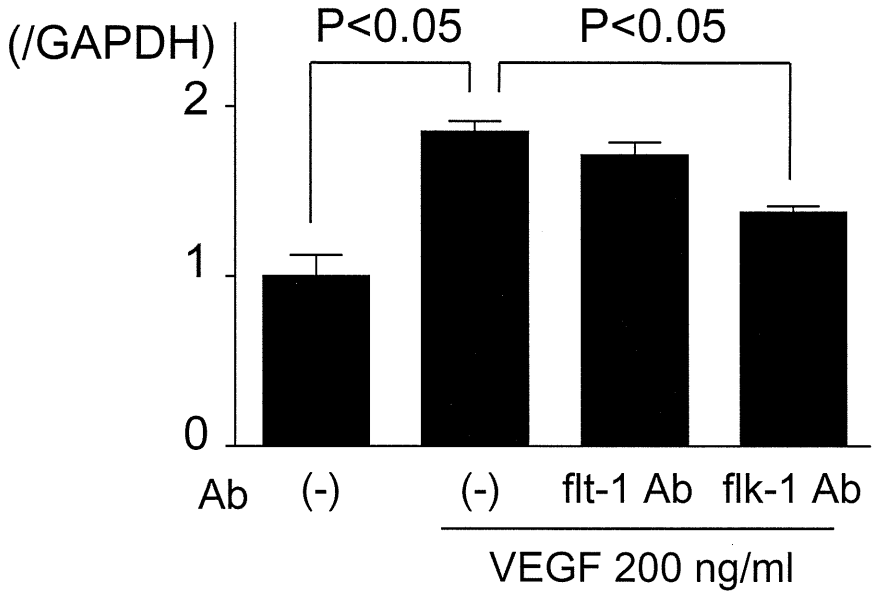

Supplemental Figure II

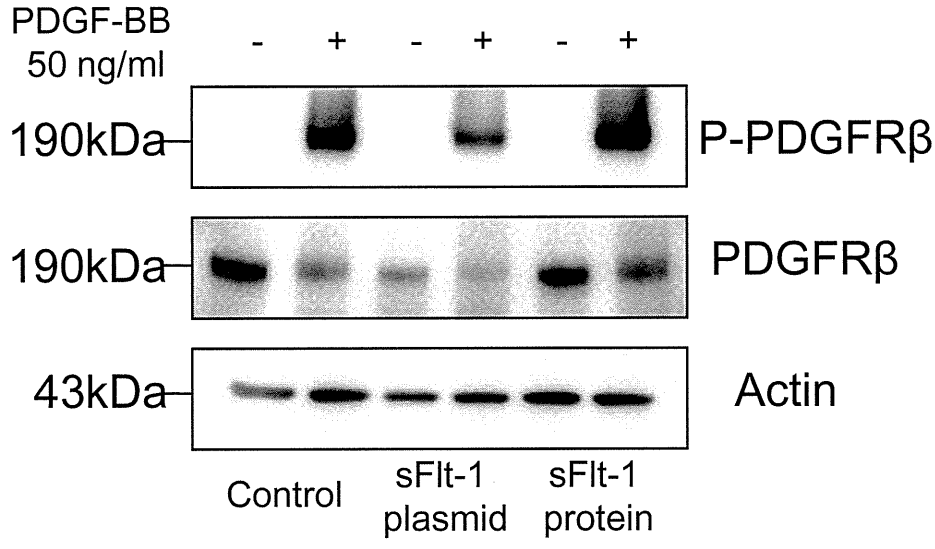

Free Radical Research, January 2009; 43(1): 37–46

informa
healthcare

Time-dependent changes of myocardial and systemic oxidative stress are dissociated after myocardial infarction

TAKAHIRO INOUE[1], TOMOMI IDE[1], MAYUMI YAMATO[2], MASAYOSHI YOSHIDA[1], TAKAKI TSUTSUMI[1], MAKOTO ANDOU[1], HIDEO UTSUMI[3], HIROYUKI TSUTSUI[4], & KENJI SUNAGAWA[1]

[1]*Department of Cardiovascular Medicine, Graduate School of Medical Sciences,* [2]*Department of REDOX Medicinal Science,* [3]*Department of Bio-functional Science, Graduate School of Pharmaceutical Sciences, Kyushu University, Fukuoka 812-8582, Japan, and* [4]*Department of Cardiovascular Medicine, Hokkaido University Graduate School of Medicine, Sapporo 060-8638, Japan*

Accepted by Professor G. Mann

(Received 10 July 2008; revised 17 September 2008)

Abstract
Reactive oxygen species (ROS) is increased in myocardium after myocardial infarction (MI), which may play a causal role in cardiac remodelling. However, there is scant direct and longitudinal evidence that systemic oxidative stress is enhanced accompanying an increase of ROS in myocardium. The authors conducted a comprehensive investigation of ROS markers by simultaneously sampling urine, blood and myocardium and *in vivo* ESR for the heart at different stages of post-MI cardiac remodelling in mouse with permanent occlusion of left coronary artery. Systemic oxidative markers increased at early days after MI and were normalized later. In contrast, TBARS and 4-hexanoyl-Lys staining were increased in non-infarct myocardium at day 28. The enhancement of ESR signal decay of methoxycarbonyl-PROXYL measured at the chest was associated with the progression of left ventricle dilatation and dysfunction. This study provided the direct evidence that redox alteration and production of ROS occurred in myocardium during the progression of cardiac remodelling and failure; however, ROS marker levels in blood and urine do not reflect the production of ROS from failing myocardium.

Keywords: *Myocardial remodelling, oxidative stress markers, heart failure, in vivo ESR*

Abbreviations: *LV, left ventricular; MI, myocardial infarction; HF, heart failure; RAS, renin-angiotensin system; ROS, reactive oxygen species; MMP, matrix metalloproteinase; TBARS, thiobarbituric acid reactive substances; 8-OH-dG, 8-hydroxy-2′-deoxyguanosine; GPx, glutathione peroxidase; SOD, superoxide dismutase; HEL, Nε-(Hexanoyl) Lysin; ESR, electron spin resonance; FS, fractional shortening; HR, heart rate; LVEDD, left ventricular end-diastolic dimension; LVESD, left ventricular end-systolic dimension; 3-methoxycarbonyl-PROXYL, 3-methoxycarbonyl-2,2,5,5-tetramethylpyrrolidine-1-oxyl*

Introduction

Pathological left ventricular (LV) remodelling after myocardial infarction (MI) is increasingly recognized as the major cause of heart failure (HF) [1]. MI induces alterations of LV architecture with scar formation, ventricular dilatation and hypertrophy of the non-infarct myocardium [2]. In the process of remodelling, activation of various neurohumoral factors and inflammatory response, including activation of the

Correspondence: Tomomi Ide, MD, PhD, Department of Cardiovascular Medicine, Kyushu University Graduate School of Medicine, 3-1-1, Maidashi, Higashi-ku, Fukuoka 812-8582, Japan. Tel: +81-92-642-5360. Fax: +81-92-642-5374. Email: tomomi_i@cardiol.med.kyushu-u.ac.jp

ISSN 1071-5762 print/ISSN 1029-2470 online
DOI: 10.1080/10715760802534820

renin-angiotensin system (RAS), contributes to healing and scar formation in the infarct myocardium. At the end of the repairing process, cardiac hypertrophy due to haemodynamic overload is associated with hypertrophic growth of cardiomyocytes accompanying fibrosis and inappropriate interstitial collagen formation. The prognosis of HF remains poor even with wide use of RAS inhibitors and β adrenergic receptor blockers [3]. Recently, growing evidence has suggested that reactive oxygen species (ROS) are involved in the pathophysiology of myocardial remodelling and failure [4–10] and increases of ROS have been shown in various animal models of HF. We and others have demonstrated that generation of ROS is increased in post-MI myocardium in mice [9] and that treatment with antioxidants or over-expression of antioxidant enzymes prevents cardiac remodelling [11–13], resulting in improvement of survival after MI [12,13]. *In vitro* experiments demonstrated that ROS mediate hypertrophy in cardiomyocytes induced by neurohumoral factors such as angiotensin II and catecholamines, as well as cytokines including TNFα [14–17]. ROS modulate extracellular matrix function via their effects on fibroblast proliferation and collagen synthesis, involving redox-sensitive activation of matrix metalloproteinases (MMPs) [11,18,19]. Moreover, ROS alter gene expression in the case of intracellular Ca^{2+} overload, activating various proteases and promoting apoptosis in cardiomyocytes [20,21]. The above findings thus strongly suggest that redox regulation may be a potential therapeutic strategy for cardiac remodelling and HF. However, despite much discussion on the biological activities of ROS in remodelling, there is scanty clinical or animal experimental evidence for elevation of systemic oxidative biomarkers corresponding to the increase of ROS in the remodelling myocardium. We thus examined the time courses of oxidative stress in the post-MI myocardium and in systemic circulation by performing simultaneous sampling of urine, blood and myocardium during the post-MI course in a HF mouse model. Since the effects of ROS depend on a balance between the pro-oxidant molecules generated and the antioxidant reserve *in vivo*, both components should be tested to obtain better understanding of the effects of ROS on the progression of remodelling. For a comprehensive investigation of oxidative stress, we measured the byproducts of ROS represented by thiobarbituric acid reactive substances (TBARS) and 8-hydroxy-2′-deoxyguanosine (8-OH-dG), as well as the antioxidant defense capacity indicated by scavenger enzymes. Moreover, excised biological specimens only enable one to identify the target of ROS after the exposure to ROS but not to reflect the dynamic changes of redox status *in vivo* in the chronic HF model. Accordingly, we applied *in vivo* ESR to estimate redox status non-invasively in the process of remodelling using a post-MI HF model in mice.

Materials and methods

Animal model

This experiment conformed with the Guide for the Care and Use of Laboratory Animals published by the US National Institute of Health and was reviewed and approved by the Committee of the Ethics on Animal Experiment, Kyushu University Graduate School of Medical Sciences, and performed in compliance with the relevant Law (No. 105) and Notification (No. 6) of the Japanese Government.

Six week-old CD-1 male mice were purchased from Kyudo Co., Ltd. (Saga, Japan). The mice were housed in a temperature- and humidity-controlled room. MI was experimentally induced in mice by ligating the left coronary artery permanently, as previously reported [11]. The mice were assigned randomly into five groups; post-MI days 1, 4, 7, 14 and 28, and the survived mice (survived/operated: $n = 6/7$, 6/8, 10/14, 9/11, 14/21, respectively) were used in the experiments on the assigned days. Urine, blood and myocardium samples were collected from each mouse. The myocardial samples of all six mice on post-MI day 4 and six mice on post-MI day 28 were examined immunohistochemically, while the samples of the other mice were used for biochemical analysis. The data were compared with those from control mice that underwent sham operation without coronary artery ligation at day 28 ($n = 7$).

Echocardiography and haemodynamic measurements

Echocardiographic studies were performed under light anaesthesia by an intraperitoneal injection of sodium pentobarbital, with spontaneous respiration before the animal was euthanized. A 2D parasternal short-axis view of the LV was obtained by applying the transducer lightly to the mid-upper left anterior chest wall. The transducer was then gently moved cephalad or caudad and angulated until desirable images were obtained. After ensuring that the image was on axis (based on roundness of the LV cavity), 2D targeted M-mode tracings were recorded at a paper speed of 50 mm/s. Our previous study showed small intra-observer and inter-observer variabilities of our echocardiographic measurements for LV dimensions and high reproducibility of measurements made in the same animals on separate days [22]. Under the same anaesthesia with Avertin, a 1.4 Fr micromanometer-tipped catheter (Millar Instruments) was inserted into the right carotid artery and then advanced into the LV for the measurement of LV pressures for the assessment of severity of HF at day 28 after MI.

Blood sampling

Blood sample was collected with 1:500 dilution of heparin just before euthanizing each animal. Plasma was separated by centrifugation at $1000 \times g$ for 15 min at 4°C and stored at −80°C until analysis. The erythrocyte fraction was washed three times with isotonic NaCl. A stock haemolysate was prepared by the addition of the 2-mercaptoethanol-EDTA stabilizing solution. The concentrated haemolysate was diluted with 2% ethanol immediately before assay.

TBARS in plasma and 8-OH-dG in urine

To assess the level of systemic oxidative stress generated in the process of cardiac remodelling after MI, we measured TBARS in plasma and 8-OH-dG in urine. Plasma TBARS was measured by fluorometric analysis. The plasma was pre-treated with 10% phosphotungstic acid and 1/12 N sulphuric acid. The sample was mixed with a reagent to obtain a final concentration of 7.5% acetic acid, 2 mmol/L EDTA and 0.4% SDS and then reacted with 0.3% thiobarbituric acid (TBA) in a boiling water bath for 45 min. After cooling, the chromogen was extracted in n-butanol/pyridine (15:1, v/v). Fluorescence of the supernatant was measured at excitation and emission wavelengths of 510 and 550 nm, respectively, using a GENios Pro™ (Tecan Group Ltd. Durham, NC). The standard was prepared using 1,1,3,3, -tetraethoxypropane (TEP).

Urine samples were collected in individual metabolic cages (Nalgen, Rochester, NY). After overnight fasting, urine sample was collected from each mouse. Urine 8-OH-dG concentration was determined using a competitive ELISA kit (8-OH-dG check®, Japan, Institute for the Control of Aging, Nagoya, Japan). The value was corrected by urinary creatinine measured with a colorimetric assay kit (Sigma, St. Louis, MO).

TBARS in myocardial tissue

The myocardium was homogenized in 10 volumes of 50 mmol/L sodium phosphate buffer at 4°C for the assay of TBARS in myocardium. The homogenate was centrifuged at $4500 \times g$ for 15 min and the supernatant was used for the biochemical assay of TBARS as in plasma.

Antioxidant enzyme activities in myocardium

To determine the change in capacity of defense during the progression of cardiac remodelling, we measured the levels of antioxidant enzyme activities in the myocardium.

The enzymatic activities of glutathione peroxidase (GPx) and superoxide dismutase (SOD) were measured spectrophotometrically (Tecan Group Ltd., GENios). GPx activity was determined according to the method of Yamamoto and Takahashi [23] by following the oxidation of NADPH in the presence of GR (Oriental Yeast Co., Ltd. Tokyo, Japan), which catalyses the reduction of oxidized glutathione (GSSH) formed by GPx. One enzyme unit is defined as the amount of enzyme that oxidizes 1 μmol of NADPH per minute. SOD activity was examined by the cytochrome c method, in which xanthine and xanthine oxidase (Oriental Yeast Co., Ltd. Tokyo, Japan) were used as a source of superoxide. A unit was defined as the quantity of SOD required for 50% inhibition of the rate of cytochrome c reduction (Wako Pure Chemical Industries, Inc. Osaka, Japan). Protein concentration was determined by the Bradford assay.

Hexanoyl-Lysine adduct (HEL) immunostaining in myocardial tissue

Left ventricular myocardial sections obtained from mice at baseline, day 3 and 28 after MI were immunolabelled by a specific monoclonal anti-HEL antibody (Nikkenn SEIL Corp.). Paraffin-embedded tissue sections (5-μm thick) were deparaffinized with xylene, refixed in Bouin's solution for 20 min, immersed in PBS, incubated with 0.3% H_2O_2 in methanol for 30 min, followed by blocking with M.O.M. mouse IgG blocking reagent. The sections were further incubated with monoclonal anti-HEL antibody in M.O.M. Diluent. After rinsing with 10 mmol/L PBS, they were incubated with biotin-labelled goat anti-rabbit IgG anti-serum (1:100 dilution; DAKO A/S) for 60 min and then with avidin-biotin complex (1:100 dilution; Vectastain ABC kit) for 60 min. After rinsing, the sections were finally incubated with 0.02% 3,3-diaminobenzidine and 0.03% H_2O_2 in deionized water for 6–9 min. As a negative control, sections were incubated with normal rabbit serum instead of anti-HEL antibody.

In vivo *electron spin resonance study*

A spin probe, 3-methoxycarbonyl-2,2,5,5-tetramethylpyrrolidine-1-oxyl (methoxycarbonyl-PROXYL) was synthesized as described previously [24]. For the *in vivo* ESR measurements, 100 mmol/L isotonic methoxycarbonyl-PROXYL was administered (3 μl/g body weight) in mice intravenously. Then ESR spectra were taken at regular intervals using a L-band ESR spectrometer (JEOL Co. Ltd., Akishima, Japan) with a loop-gap resonator (33 mm i.d. and 30 mm in length), as reported previously [25,26]. The power of the 1.1 GHz microwave was 10 mW. The amplitude of the 100-kHz field modulation was 0.063 mT. The signal decay rates, which were used as an index of ROS generation, were determined from the semi-logarithmic plots of signal

intensity vs time after probe injection. Tiron or dimethylthiourea (DMTU) (3 μmol/mouse, dissolved in saline) was administered simultaneously with the probe to confirm the relationship between the signal decay and ROS generation.

Statistical analysis

All data are expressed as mean ± SEM. Between-group comparisons of the means were performed by one-way ANOVA followed by *t*-tests. Bonferroni's correction was done for multiple comparisons of means. A *p*-value less than 0.05 was considered to be statistically significant.

Results

Animal characteristics

The echocardiographic data of surviving mice at days 1, 4, 7, 14 and 28 after MI and control mice are shown in Table I. LV diameters were significantly greater in MI mice at day 4 and thereafter compared to sham-operated control mice. Moreover, MI mice had smaller fractional shortening and anterior wall thickness. There were no alterations in LV diameter and systolic function in sham-operated mice without coronary artery ligation up to day 28 after the operation (data not shown). At day 28, left ventricule LV end-diastolic pressure (LVEDP) was increased in MI (2.6 ± 0.7 vs 14.0 ± 2.3, $p < 0.01$) and LV weight (wt)/body wt (3.12 ± 0.11 vs 3.68 ± 0.17 mg/g, $p < 0.05$), RV wt/body wt (0.88 ± 0.06 vs 1.38 ± 0.11 mg/g, $p < 0.05$), lung wt/body wt (5.36 ± 0.13 vs 7.71 ± 0.80 mg/g, $p < 0.05$) were all increased in MI. The prevalence of pleural effusion was significantly higher in MI (0 vs 50%, $p < 0.01$).

Oxidative byproducts in plasma and urine

Plasma TBARS and urinary 8-OH-dG were significantly elevated at day 1 after MI (Figure 1), and declined to control levels at day 7 and thereafter.

Oxidative markers and antioxidant enzyme activity in myocardial tissue

We measured TBARS (an indicator of lipid peroxidation) and performed immunohistochemical staining of HEL in both infarct and non-infarct myocardial samples. In the infarct area, TBARS increased at day 1 and 7 after MI (Figure 2A). In the non-infarct area, on the contrary, TBARS level was not altered in the early days (days 1, 7 and 14) after MI but was elevated only at day 28.

In agreement with the results of myocardial TBARS, HEL-positive cardiomyocytes were located in the infarct area, whereas there was no staining in the non-infarct area at day 4. (Figure 3). HEL is a novel lipid hydroperoxide modified lysine residue, which is formed by oxidative modification by oxidized ω6 fatty acids such as linoleic acid or arachidonic acid. HEL is a useful biomarker for the initial stage of lipid peroxidation. Although positive staining lasted in the infarct area at day 28, the myocardium was mostly replaced by fibrous tissue and little living myocyte existed. In the non-infarct area, cardiomyocytes were hypertrophied and positively stained by HEL antibody. These suggest that lipid peroxidation starts at an early stage in the infarct area but at late remodelling stage in the non-infarct area. This is consistent with TBARS level in myocardium and indicated increased generation of ROS in the non-infarct area at day 28. The increase of TBARS in the non-infarct area was associated with a significant decline in SOD activity and a tendency of decrease in GPx activity at day 28 (Figure 4).

In vivo *ESR in the heart*

Since TBARS is known to be a non-specific assay to measure lipid peroxidation from biological fluids and tissues and many other substances besides reactive aldehydes react with TBA, we used *in vivo* ESR to determine whether the level of ROS increased in the heart in the remodelling process. Methoxycarbonyl-PROXYL, a stable membrane-permeable nitroxyl radical, is converted into its non-magnetic products, such as its hydroxylamine, immediately after the

Table I. Echocardiographic data.

		Time after MI (days)				
	Control	1	4	7	14	28
n	7	6	6	10	9	8
Heart rate (bpm)	524±22	564±25	552±16	568±23	551±28	589±43
LVEDD (mm)	4.0±0.2	4.5±0.2	5.0±0.2**	5.1±0.2**	5.4±0.1**	5.6±0.2**
LVESD (mm)	2.3±0.2	3.6±0.2**	3.9±0.2**	3.9±0.1**	4.2±0.1**	4.4±0.1**
Fractional shortening (%)	37.6±1.6	21.1±1.6**	22.2±1.6**	23.2±1.6**	20.7±1.0**	21.0±2.7**
Infarct wall thickness (mm)	0.83±0.03	0.60±0.05**	0.61±0.03**	0.44±0.02**	0.44±0.06**	0.30±0.08**
Non-infarct wall thickness (mm)	0.84±0.04	0.80±0.05	1.00±0.02	1.13±0.07*	1.30±0.05**	1.25±0.18**

Control, sham-operated mice; LV, left ventiruclar; EDD, end-diastolic dimension; ESD, end-systolic dimension.
Values are means±SEM. * $p < 0.05$, ** $p < 0.01$ vs controls.

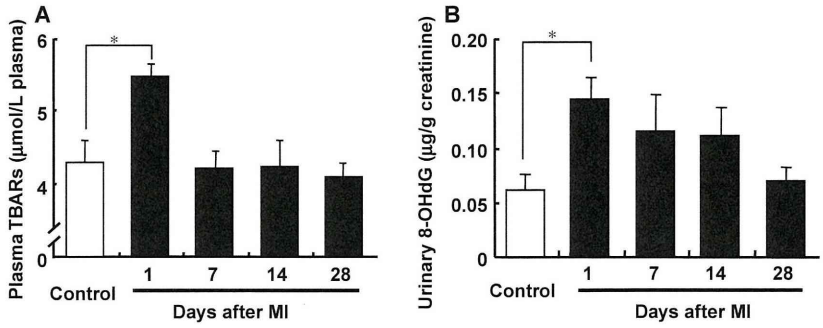

Figure 1. Time-dependent changes of plasma TBARs (A) and urinary 8-OHdG (B) in sham-operated control mice ($n=7$) and mice on day 1 ($n=6$), day 7 ($n=10$), day 14 ($n=9$) and day 28 ($n=8$) after MI. Values are means ± SEM. * $p<0.05$, ** $p<0.01$ compared with sham-operated control.

reaction with hydroxy radicals or other reductants. To determine the level of ROS or redox status by *in vivo* ESR measurements, we used methoxycarbonyl-PROXYL as a spin probe which was observed as three sharp lines by ESR spectroscopy (Figure 5A).

We applied signal decay of methoxycarbonyl-PROXYL to *in vivo* ESR to measure ROS generation non-invasively in the failing heart in mice after MI. When the ESR spectrum was measured at the chest level, the signal decay rate was greater in MI mice than sham-operated mice (Figure 5B). The increase of the signal decay observed in MI was suppressed by a simultaneous injection of antioxidants, Tiron or DMTU (Figure 5C and D), indicating the enhancement of free radical reactions at the chest in MI mice. To confirm that the enhancement of signal decay is localized at the chest and does not reflect the increase of systemic free radical generation, the same ESR measurement was repeated at the other parts of the body, head and abdomen from the same animals. ESR signal decay was similar between the two groups when the spectrum was detected at the head and abdominal levels (Figure 5E and F).

Redox alteration during the process of remodelling after MI

Using this *in vivo* ESR technique, we measured free radical production during the time course of remodelling after MI in mice. Radical generation was increased gradually in 4 weeks after MI, which was in parallel to the increase of LVEDD and LVESD and the decrease of EF assessed by echocardiography (Figure 6).

Discussion

In the post-MI myocardium, early remodelling occurs accompanied by infarct expansion, regional dilatation and thinning of the infarct zone and is followed by further deterioration in cardiac performance and increased neurohormonal activation in late remodelling. ROS play an important role in the progression of remodelling in the post-MI myocardium. However, phase-dependent alteration of ROS production in the post-MI myocardium has not been discussed. Moreover, despite a lack of evidence, it is widely misconstrued that an increase of local ROS production is reflected by increases of systemic ROS markers. The present study demonstrates that systemic elevations of ROS markers occur only at the earlier phase after MI. On the contrary, the generation of ROS in non-infarct myocardium is increased from the late phase.

Roles of ROS in the progression of cardiac remodelling

ROS potentially cause cellular damage and dysfunction. Whether the effects of ROS are beneficial or

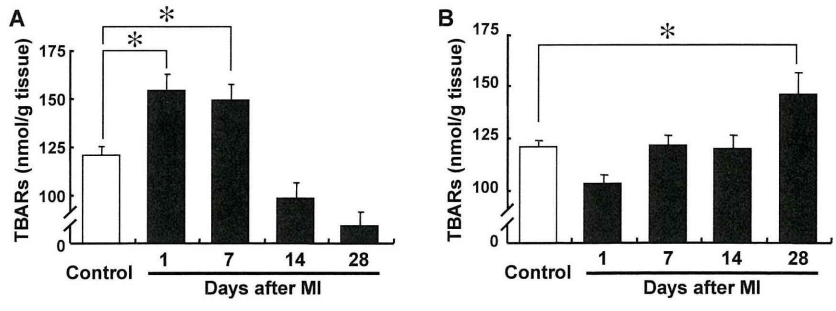

Figure 2. Time-dependent changes of TBARs in infarct (A) and in non-infarct (B) myocardium in sham-operated control ($n=7$) and on day 1 ($n=6$), day 7 ($n=10$), day 14 ($n=9$) and day 28 ($n=8$) after MI. Values are means ± SEM. * $p<0.05$ compared with sham-operated control.

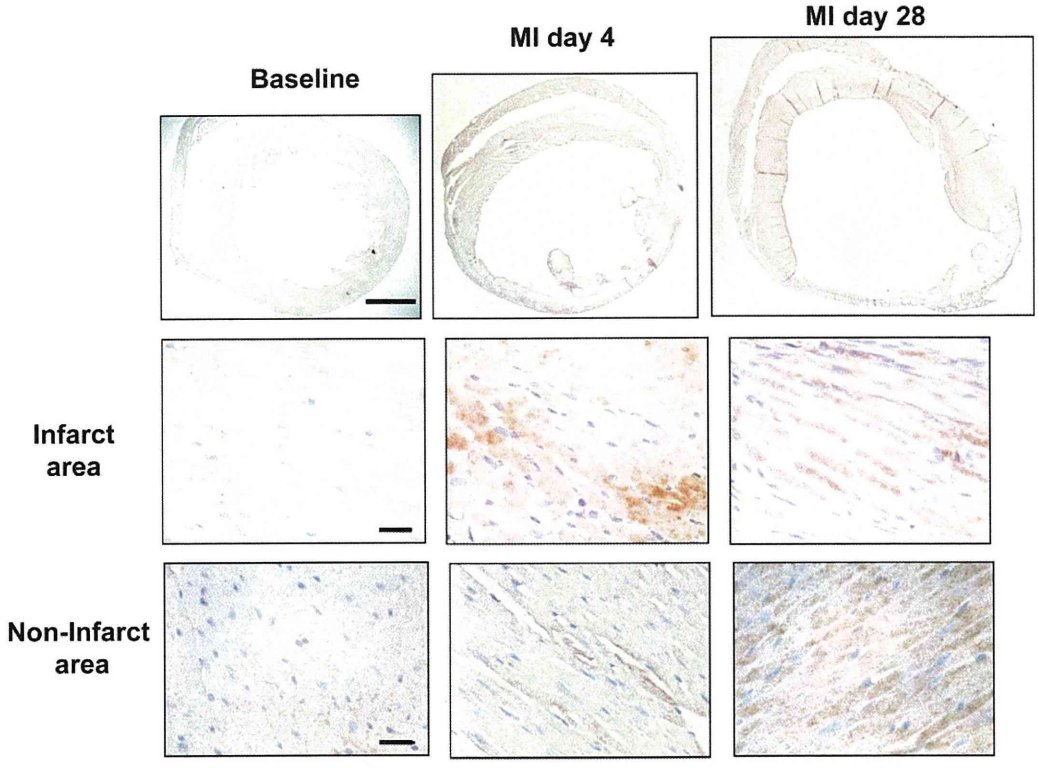

Figure 3. Immunohistochemical detection of HEL moieties in the remodelling process in whole LV, infarct myocardium and non-infarct myocardium, during acute-phase (day 4) and late-phase (day 28) after MI. Scale bar; 1 mm (top) and 10 μm (infarct area and non-infarct area).

harmful depends on the site of action, the source, the amount of ROS generation and the resulting redox balance. Several groups reported that ROS are increased in congestive HF patients [27,28] and accumulating evidence from animal studies revealed that increased ROS play a pivotal role in the pathogenesis and progression of HF [4,9,29–33]. However, whether systemic ROS markers are useful for determining the redox state of the failing heart remains unknown. Li et al. [34] used LC/MS/MS to analyse F_2-isoprostanes in urine from HF patients. They found that only a few peaks were increased, but the most abundant isomer 5-epi-8,12-iso-iP$F_{2\alpha}$-VI was comparable to control subjects. Other clinical studies examined ROS in serum or urine in HF patients by measuring redox markers and reported that ROS are elevated in functionally very poor, NYHA class III or class IV patients. At the time of acute deterioration of HF or sudden onset of cardiac ischemia, patients often have congestion or elevation of LV end diastolic pressure. In such conditions, the immune system, neurohormonal factors such as TNFα and other cytokines are activated with concurrent activation of sympathetic nerve, all of which cause endothelial damage and other organ disorders [35]. In fact, acute MI is associated with a marked increase of inflammatory cells. Previous reports have demonstrated that inflammatory responses and neurohormonal factors cause the generation of oxidative stress not only from the myocardium but also from the vasculature [36–40]. These observations are consistent with our result showing that alteration of systemic ROS markers may not always reflect ROS generation in the myocardium.

Redox status estimated by in vivo ESR

ESR spectroscopy is a useful method to estimate redox status in living animals. In this study, we demonstrated using *in vivo* ESR spectroscopy that increased generation of free radicals in the heart correlated with dilatation of LV and decrease in EF, both of which are indices of the myocardial remodelling process after MI.

There are several advantages to determine ROS generation by *in vivo* ESR spectroscopy. First, the method allows non-invasive assessment of ROS generation in an *in vivo* setting. Secondly, *in vivo* ESR can be repeated in the same animal at different time points, indicating that the ESR technique has the potential to be used as a diagnostic tool in the future. Thirdly, this ESR technique can estimate and quantify the 'net' redox state. Antioxidant enzymes and reductants (such as glutathione) in the ROS generating system together determine the total redox status in biological systems, which may change dynamically and acutely in the heart after MI. Byproducts of free oxygen radicals such as lipid

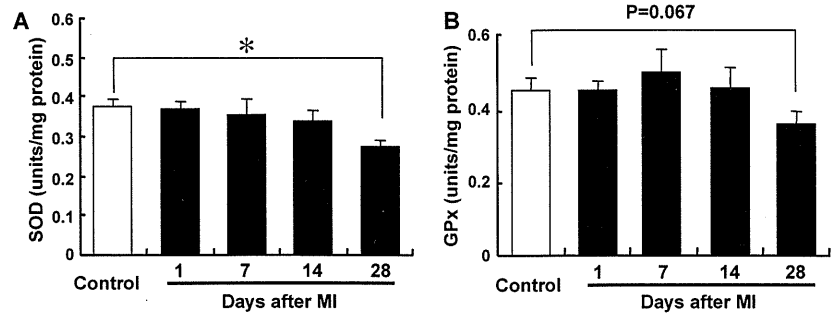

Figure 4. Time-dependent changes of activities of SOD (A) and GPx (B) in non-infarcted myocardium from sham-operated control ($n=7$) and on day 1 ($n=6$), day 7 ($n=10$), day 14 ($n=9$) and day 28 ($n=8$) after MI. Values are means ± SEM. * $p<0.05$ compared with sham-operated control.

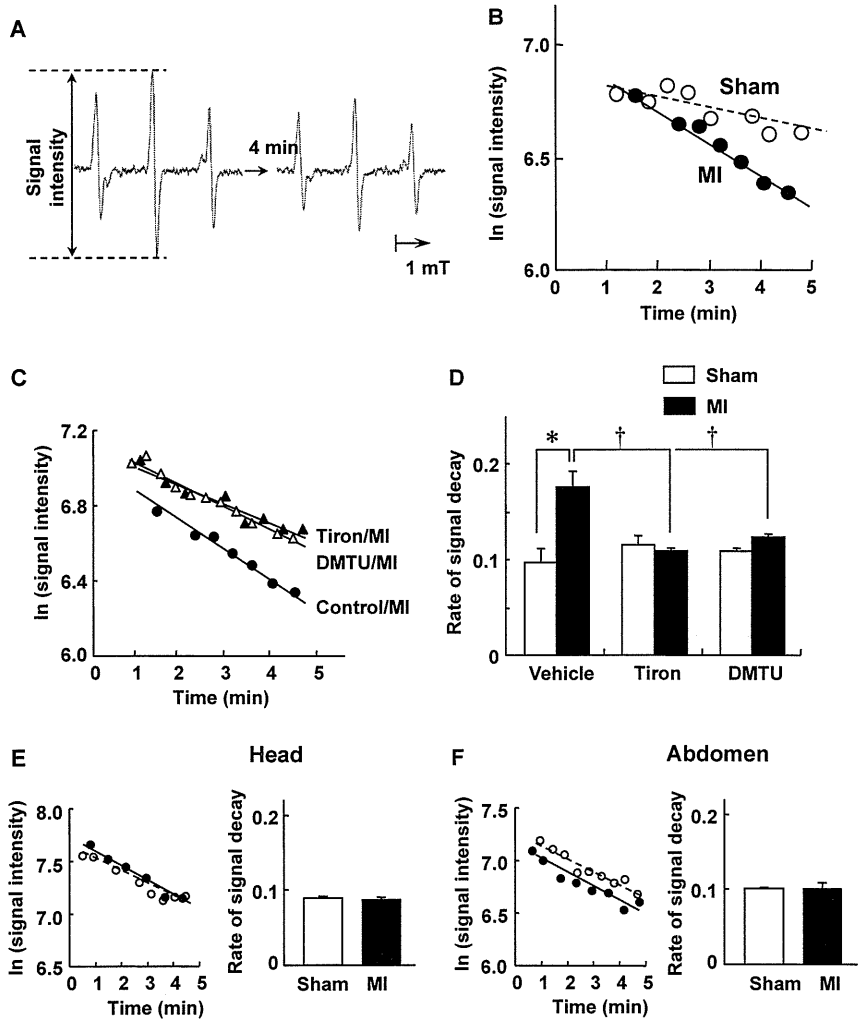

Figure 5. (A) A representative ESR signal of methoxycarbonyl-PROXYL at the chest level of a mouse with myocardial infarction (MI). (B) Semilogarithmic plots of the peak heights of the ESR spectra of methoxycarbonyl-PROXYL after spin probe injection. The signal intensity declined with time, which is defined as the signal decay. (C) The effects of addition of free radical scavengers on the rate of signal decay measured by *in vivo* ESR spectroscopy in individual MI mice. Tiron (a superoxide scavenger) or dimetylthiourea (DMTU; a hydroxyradical scavenger) was injected simultaneously with the injection of methoxycarbonyl-PROXYL. (D) Rates of signal decay measured by *in vivo* ESR in sham and MI groups in the absence and presence of radical scavengers ($n=6$ in each group). *$p<0.01$ vs sham-vehicle group and †$p<0.01$ vs MI-vehicle group. Values are means ± SEM. (E, F) Representative plots of individual mice and rates of *in vivo* ESR signal decay in sham and MI groups ($n=5$ each) measured at the head (E) and abdomen (F).

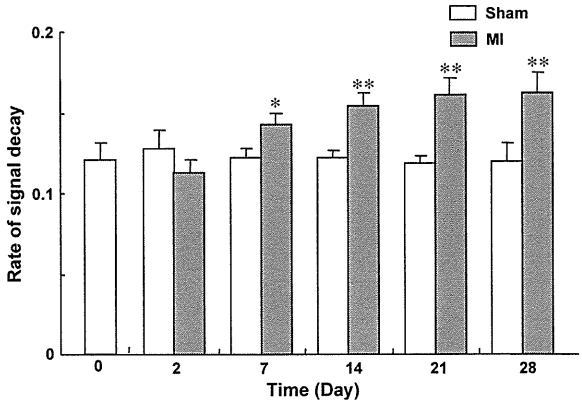

Figure 6. Changes in the rates of signal decay over time measured by *in vivo* ESR spectroscopy in sham and MI mice at days 0, 2, 7, 14 and 28 after operation ($n=7$ in each group). Values are means ±SEM. $*p<0.05$, $**p<.01$ vs sham values for the rate of signal decay.

peroxide, products of protein modifications and DNA damage do not always represent the net capacity of ROS reactions and do not necessary reflect ROS generation in specific organs or tissue. Difficulty in the interpretation of enhanced signal decay has been pointed out, because the nitroxyl radicals are known to react with not only free radicals but also other reductants including ascorbic acid and glutathione. However, we found that the increased ESR signal decay in heart failure was normalized by the addition of Tiron and DMTU. Furthermore, the TBARs study provided evidence that the ESR data reflect the increase of ROS in the failing heart, all of which support that the enhancement of signal decay in late remodelling represents at least the alteration of total redox status in the myocardium, most probably due to an increase of ROS.

Alteration of antioxidants and lipid peroxidation in non-infarct myocardium

We found that ROS markers including both byproducts of ROS and antioxidant enzymes were altered concomitantly in urine and blood at the early phase after MI and were normalized at the late remodelling state at 28 days post-MI. An increase of lipid peroxidation indicated by TBARS in infarct myocardium coincided with these systemic alterations (Figures 1 and 2). On the contrary, with the progression of remodelling represented by LV dilatation and reduced ejection fraction, the TBARS level in non-infarct myocardium increased at day 28. The immunohistochemical analysis by HEL antigen substantiated the finding that ROS was increased in the non-infarct myocardium during late remodelling. It is consistent with our previous findings in a tachycardia-induced canine HF model, in which ROS generation was enhanced in the failing myocardium and correlated with LV end-diastolic pressure and LV ejection fraction [41]. Nevertheless, it remains unknown why oxidative stress was not detectable in urine or in blood in late remodelling after MI, even with the progression of remodelling. A possible explanation is the differences in the source and amount of ROS between the early phase and the chronic phase of HF. In the later phase of post-MI remodelling, ROS increase may occur mainly in the myocardium and multiple defense mechanisms against ROS stabilize the levels in blood and urine. Moreover, ROS is so short-lived that it may not be possible to detect them in urine or blood when the source is localized in a single organ. In contrast, systemic inflammatory responses manifested clinically as leukocytosis and increased cytokines during acute deterioration or sudden ischemia [42–46] may not have enough time to cope with the acute ROS attack and redox change. We suspect that the acute increase in systemic ROS markers after MI is due to systemic activation of inflammatory cells. However, while administration of cyclophosphamide depletes leukocytes by 93% [15,47], the drug inhibited TBARS only partially by ~ 48% (data not shown). This indicates that sources other than leukocytes, such as vasculature, may contribute to systemic ROS generation in the acute phase of MI. All of these results suggest the difficulties of detecting ROS in blood or urine by specific markers in chronic HF, even with enhanced production of ROS from the remodelling myocardium.

Among the many detection techniques of ROS markers available currently, the most sensitive method is the detection of isoprostanes by mass spectroscopy. However, it is known that most of the major peaks of isoprostanes are not elevated in urine from HF patients [30]. Furthermore, commercially available ELISA kits are not as reliable as GC-MS assay [48]. Therefore, we measured a sensitive but not very specific marker TBARS for estimating ROS in plasma.

Clinical implications

Our study suggests that the increased local production of ROS is not always reflected in blood or urine during progression of remodelling. ROS are extremely unstable and difficult to detect directly. The establishment of a non-invasive method to detect ROS generated locally in the remodelling myocardium may permit time- and tissue-targeted therapy for more effective treatment of remodelling and failing heart.

Conclusion

We demonstrated that the generation of ROS in the non-infarct myocardium increases with the progression of cardiac remodelling and this increase is not

reflected by the levels of ROS markers in blood and urine. Clarification of the mechanisms of ROS-mediated remodelling and targeting non-infarct myocardium may lead to novel and effective therapeutic strategies for HF.

Acknowledgements

This study was supported in part by the Uehara memorial foundation and grants from the Ministry of Education (181-00006). A part of this study was conducted in Kyushu University Station for Collaborative Research II.

***Declaration of interest*:** The authors report no conflicts of interest. The authors alone are responsible for the content and writing of the paper.

References

[1] Gheorghiade M, Bonow RO. Chronic heart failure in the United States: a manifestation of coronary artery disease. Circulation 1998;97:282–289.

[2] Cohn JN, Ferrari R, Sharpe N. Cardiac remodeling—concepts and clinical implications: a consensus paper from an international forum on cardiac remodeling. Behalf of an International Forum on Cardiac Remodeling. J Am Coll Cardiol 2000;35:569–582.

[3] Liew CC, Dzau VJ. Molecular genetics and genomics of heart failure. Nat Rev Genet 2004;5:811–825.

[4] Tsutsui H, Ide T, Hayashidani S, Kinugawa S, Suematsu N, Utsumi H, Takeshita A. Effects of ACE inhibition on left ventricular failure and oxidative stress in Dahl salt-sensitive rats. J Cardiovasc Pharmacol 2001;37:725–733.

[5] Ichihara S, Yamada Y, Ichihara G, Kanazawa H, Hashimoto K, Kato Y, Matsushita A, Oikawa S, Yokota M, Iwase M. Attenuation of oxidative stress and cardiac dysfunction by bisoprolol in an animal model of dilated cardiomyopathy. Biochem Biophys Res Commun 2006;350:105–113.

[6] Mollnau H, Oelze M, August M, Wendt M, Daiber A, Schulz E, Baldus S, Kleschyov AL, Materne A, Wenzel P, Hink U, Nickenig G, Fleming I, Munzel T. Mechanisms of increased vascular superoxide production in an experimental model of idiopathic dilated cardiomyopathy. Arterioscler Thromb Vasc Biol 2005;25:2554–2559.

[7] Shite J, Qin F, Mao W, Kawai H, Stevens SY, Liang C. Antioxidant vitamins attenuate oxidative stress and cardiac dysfunction in tachycardia-induced cardiomyopathy. J Am Coll Cardiol 2001;38:1734–1740.

[8] Carlberg I, Mannervik B. Purification and characterization of the flavoenzyme glutathione reductase from rat liver. J Biol Chem 1975;250:5475–5480.

[9] Ide T, Tsutsui H, Kinugawa S, Suematsu N, Hayashidani S, Ichikawa K, Utsumi H, Machida Y, Egashira K, Takeshita A. Direct evidence for increased hydroxyl radicals originating from superoxide in the failing myocardium. Circ Res 2000;86:152–157.

[10] Lang D, Mosfer SI, Shakesby A, Donaldson F, Lewis MJ. Coronary microvascular endothelial cell redox state in left ventricular hypertrophy: the role of angiotensin II. Circ Res 2000;86:463–469.

[11] Kinugawa S, Tsutsui H, Hayashidani S, Ide T, Suematsu N, Satoh S, Utsumi H, Takeshita A. Treatment with dimethylthiourea prevents left ventricular remodeling and failure after experimental myocardial infarction in mice: role of oxidative stress. Circ Res 2000;87:392–398.

[12] Shiomi T, Tsutsui H, Matsusaka H, Murakami K, Hayashidani S, Ikeuchi M, Wen J, Kubota T, Utsumi H, Takeshita A. Overexpression of glutathione peroxidase prevents left ventricular remodeling and failure after myocardial infarction in mice. Circulation 2004;109:544–549.

[13] Matsushima S, Kinugawa S, Ide T, Matsusaka H, Inoue N, Ohta Y, Yokota T, Sunagawa K, Tsutsui H. Overexpression of glutathione peroxidase attenuates myocardial remodeling and preserves diastolic function in diabetic heart. Am J Physiol Heart Circ Physiol 2006;291:H2237–H2245.

[14] Suematsu N, Tsutsui H, Wen J, Kang D, Ikeuchi M, Ide T, Hayashidani S, Shiomi T, Kubota T, Hamasaki N, Takeshita A. Oxidative stress mediates tumor necrosis factor-alpha-induced mitochondrial DNA damage and dysfunction in cardiac myocytes. Circulation 2003;107:1418–1423.

[15] Machida Y, Kubota T, Kawamura N, Funakoshi H, Ide T, Utsumi H, Li YY, Feldman AM, Tsutsui H, Shimokawa H, Takeshita A. Overexpression of tumor necrosis factor-alpha increases production of hydroxyl radical in murine myocardium. Am J Physiol Heart Circ Physiol 2003;284:H449–H455.

[16] Foo RS, Siow RC, Brown MJ, Bennett MR. Heme oxygenase-1 gene transfer inhibits angiotensin II-mediated rat cardiac myocyte apoptosis but not hypertrophy. J Cell Physiol 2006;209:1–7.

[17] Nakagami H, Takemoto M, Liao JK. NADPH oxidase-derived superoxide anion mediates angiotensin II-induced cardiac hypertrophy. J Mol Cell Cardiol 2003;35:851–859.

[18] Siwik DA, Chang DL, Colucci WS. Interleukin-1beta and tumor necrosis factor-alpha decrease collagen synthesis and increase matrix metalloproteinase activity in cardiac fibroblasts *in vitro*. Circ Res 2000;86:1259–1265.

[19] Siwik DA, Pagano PJ, Colucci WS. Oxidative stress regulates collagen synthesis and matrix metalloproteinase activity in cardiac fibroblasts. Am J Physiol Cell Physiol 2001;280:C53–C60.

[20] Matsushima S, Ide T, Yamato M, Matsusaka H, Hattori F, Ikeuchi M, Kubota T, Sunagawa K, Hasegawa Y, Kurihara T, Oikawa S, Kinugawa S, Tsutsui H. Overexpression of mitochondrial peroxiredoxin-3 prevents left ventricular remodeling and failure after myocardial infarction in mice. Circulation 2006;113:1779–1786.

[21] Pimentel DR, Amin JK, Xiao L, Miller T, Viereck J, Oliver-Krasinski J, Baliga R, Wang J, Siwik DA, Singh K, Pagano P, Colucci WS, Sawyer DB. Reactive oxygen species mediate amplitude-dependent hypertrophic and apoptotic responses to mechanical stretch in cardiac myocytes. Circ Res 2001;89:453–460.

[22] Shiomi T, Tsutsui H, Hayashidani S, Suematsu N, Ikeuchi M, Wen J, Ishibashi M, Kubota T, Egashira K, Takeshita A. Pioglitazone, a peroxisome proliferator-activated receptor-gamma agonist, attenuates left ventricular remodeling and failure after experimental myocardial infarction. Circulation 2002;106:3126–3132.

[23] Yamamoto Y, Takahashi K. Glutathione peroxidase isolated from plasma reduces phospholipid hydroperoxides. Arch Biochem Biophys 1993;305:541–545.

[24] Sano H, Matsumoto K, Utsumi H. Synthesis and imaging of blood-brain-barrier permeable nitroxyl-probes for free radical reactions in brain of living mice. Biochem Mol Biol Int 1997;42:641–647.

[25] Han JY, Takeshita K, Utsumi H. Noninvasive detection of hydroxyl radical generation in lung by diesel exhaust particles. Free Radic Biol Med 2001;30:516–525.

[26] Phumala N, Ide T, Utsumi H. Noninvasive evaluation of *in vivo* free radical reactions catalyzed by iron using *in vivo* ESR spectroscopy. Free Radic Biol Med 1999;26:1209–1217.
[27] Belch JJ, Bridges AB, Scott N, Chopra M. Oxygen free radicals and congestive heart failure. Br Heart J 1991;65:245–248.
[28] Dieterich S, Bieligk U, Beulich K, Hasenfuss G, Prestle J. Gene expression of antioxidative enzymes in the human heart: increased expression of catalase in the end-stage failing heart. Circulation 2000;101:33–39.
[29] Ide T, Tsutsui H, Hayashidani S, Kang D, Suematsu N, Nakamura K, Utsumi H, Hamasaki N, Takeshita A. Mitochondrial DNA damage and dysfunction associated with oxidative stress in failing hearts after myocardial infarction. Circ Res 2001;88:529–535.
[30] Cargnoni A, Ceconi C, Bernocchi P, Boraso A, Parrinello G, Curello S, Ferrari R. Reduction of oxidative stress by carvedilol: role in maintenance of ischaemic myocardium viability. Cardiovasc Res 2000;47:556–566.
[31] Guo P, Nishiyama A, Rahman M, Nagai Y, Noma T, Namba T, Ishizawa M, Murakami K, Miyatake A, Kimura S, Mizushige K, Abe Y, Ohmori K, Kohno M. Contribution of reactive oxygen species to the pathogenesis of left ventricular failure in Dahl salt-sensitive hypertensive rats: effects of angiotensin II blockade. J Hypertens 2006;24:1097–1104.
[32] Miwa S, Toyokuni S, Nishina T, Nomoto T, Hiroyasu M, Nishimura K, Komeda M. Spaciotemporal alteration of 8-hydroxy-2′-deoxyguanosine levels in cardiomyocytes after myocardial infarction in rats. Free Radic Res 2002;36:853–858.
[33] Zhang GX, Kimura S, Nishiyama A, Shokoji T, Rahman M, Yao L, Nagai Y, Fujisawa Y, Miyatake A, Abe Y. Cardiac oxidative stress in acute and chronic isoproterenol-infused rats. Cardiovasc Res 2005;65:230–238.
[34] Li H, Lawson JA, Reilly M, Adiyaman M, Hwang SW, Rokach J, FitzGerald GA. Quantitative high performance liquid chromatography/tandem mass spectrometric analysis of the four classes of F(2)-isoprostanes in human urine. Proc Natl Acad Sci USA 1999;96:13381–13386.
[35] Agnoletti L, Curello S, Bachetti T, Malacarne F, Gaia G, Comini L, Volterrani M, Bonetti P, Parrinello G, Cadei M, Grigolato PG, Ferrari R. Serum from patients with severe heart failure downregulates eNOS and is proapoptotic: role of tumor necrosis factor-alpha. Circulation 1999;100:1983–1991.
[36] Kunsch C, Medford RM. Oxidative stress as a regulator of gene expression in the vasculature. Circ Res 1999;85:753–766.
[37] Al-Mehdi AB, Zhao G, Dodia C, Tozawa K, Costa K, Muzykantov V, Ross C, Blecha F, Dinauer M, Fisher AB. Endothelial NADPH oxidase as the source of oxidants in lungs exposed to ischemia or high K+. Circ Res 1998;83:730–737.
[38] Iuchi T, Akaike M, Mitsui T, Ohshima Y, Shintani Y, Azuma H, Matsumoto T. Glucocorticoid excess induces superoxide production in vascular endothelial cells and elicits vascular endothelial dysfunction. Circ Res 2003;92:81–87.
[39] Bertuglia S, Giusti A. Microvascular oxygenation, oxidative stress, NO suppression and superoxide dismutase during postischemic reperfusion. Am J Physiol Heart Circ Physiol 2003;285:H1064–H1071.
[40] Taniyama Y, Griendling KK. Reactive oxygen species in the vasculature: molecular and cellular mechanisms. Hypertension 2003;42:1075–1081.
[41] Aebi H. Catalase *in vitro*. Methods Enzymol 1984;105:121–126.
[42] Nakamura H, Takata S, Umemoto S, Matsuzaki M. Induction of left ventricular remodeling and dysfunction in the recipient heart following donor heart myocardial infarction: new insights into the pathological role of tumor necrosis factor-alpha from a novel heterotopic transplant-coronary ligation model. J Cardiol 2003;41:41–42.
[43] Maury CP. Monitoring the acute phase response: comparison of tumour necrosis factor (cachectin) and C-reactive protein responses in inflammatory and infectious diseases. J Clin Pathol 1989;42:1078–1082.
[44] Guillen I, Blanes M, Gomez-Lechon MJ, Castell JV. Cytokine signaling during myocardial infarction: sequential appearance of IL-1 beta and IL-6. Am J Physiol 1995;269:R229–R235.
[45] Basaran Y, Basaran MM, Babacan KF, Ener B, Okay T, Gok H, Ozdemir M. Serum tumor necrosis factor levels in acute myocardial infarction and unstable angina pectoris. Angiology 1993;44:332–337.
[46] Marx N, Neumann FJ, Ott I, Gawaz M, Koch W, Pinkau T, Schomig A. Induction of cytokine expression in leukocytes in acute myocardial infarction. J Am Coll Cardiol 1997;30:165–170.
[47] Fine PE. Implications of different study designs for the evaluation of acellular pertussis vaccines. Dev Biol Stand 1997;89:123–133.
[48] Pratico D, Lawson JA, Rokach J, FitzGerald GA. The isoprostanes in biology and medicine. Trends Endocrinol Metab 2001;12:243–247.

This paper was first published online on iFirst on 1 December 2008.

Bionic Cardiology: Exploration Into a Wealth of Controllable Body Parts in the Cardiovascular System

Masaru Sugimachi, *Member, IEEE*, and Kenji Sunagawa, *Senior Member, IEEE*

Clilnical Application Review

Abstract—**Bionic cardiology is the medical science of exploring electronic control of the body, usually via the neural system. Mimicking or modifying biological regulation is a strategy used to combat diseases. Control of ventricular rate during atrial fibrillation by selective vagal stimulation, suppression of ischemia-related ventricular fibrillation by vagal stimulation, and reproduction of neurally commanded heart rate are some examples of bionic treatment for arrhythmia. Implantable radio-frequency-coupled on-demand carotid sinus stimulators succeeded in interrupting or preventing anginal attacks but were replaced later by coronary revascularization. Similar but fixed-intensity carotid sinus stimulators were used for hypertension but were also replaced by drugs. Recently, however, a self-powered implantable device has been reappraised for the treatment of drug-resistant hypertension. Closed-loop spinal cord stimulation has successfully treated severe orthostatic hypotension in a limited number of patients. Vagal nerve stimulation is effective in treating heart failure in animals, and a small-size clinical trial has just started. Simultaneous corrections of multiple hemodynamic abnormalities in an acute decompensated state are accomplished simply by quantifying fundamental cardiovascular parameters and controlling these parameters. Bionic cardiology will continue to promote the development of more sophisticated device-based therapies for otherwise untreatable diseases and will inspire more intricate applications in the twenty-first century.**

Index Terms—**Biological regulation, feedback control, implantable device, nerve stimulation, system identification.**

I. Introduction

BIONIC cardiology can be defined as medical science in the field of cardiovascular medicine, which explores the electronic control of the body [1], [2]. The term "bionic" derives literally from "bio" (meaning life) and "-onic" (short for electronic). Utilizing the biological amplification mechanism of excitable membranes is an ingenious way to save power and ensure long-term operation of electronic devices. Therefore, the electronic controllers are usually designed to act on specialized tissues such as nerves, skeletal muscles, and myocardium. Since the neural system acts as the control center of the biological regulatory systems, the most efficient way of intervening and controlling the body is to manipulate the neural system.

In the earlier studies of our groups, we defined bionic cardiology in a narrower sense. In developing methods to artificially reconstruct functional defects such as severe orthostatic hypotension (due to loss of pressure stabilization function), we attempted to mimic the biological regulation as precisely as possible [3]–[6] (Fig. 1). To accomplish this, we applied the white-noise approach to unveil the detailed characteristics of complexly integrated biological regulation [4], [7]–[14]. Therefore, by "bionic" cardiology, we meant the reproduction of biological regulation. Although it is not always true (see below), through our efforts in reproducing biological regulation, we began to take full advantage of control engineering in developing artificial controllers. This breakthrough made it possible for us to design feedback closed-loop control rather than open-loop control to achieve therapeutic goals.

Later, we learned that only mimicking biological regulation is not sufficient in treating common diseases. Our body is often affected by common diseases despite the presence of normally functioning biological regulation. In other words, under certain pathophysiological conditions, the normal biological regulation fails to accommodate disease conditions. In some diseases such as heart failure, the biological regulation system may in fact participate in the process of disease evolution and progression. This is best illustrated by the fact that heart failure can be treated with drugs that antagonize biological regulation. Therefore, the strategy to combat these "common" diseases should go beyond the restoration of normal biological regulation. We do not have any model at hand to learn from. In treating common diseases, one has to modify the biological regulation rather than to mimic physiological regulation.

In this paper, we attempt to discuss bionic cardiology in a broader sense, for the reason mentioned above. We also include some earlier studies of open-loop or on-demand control; these examples may serve as a basis for the development of more sophisticated feedback controllers by contemporary control engineering. How we choose short-term therapeutic targets for the feedback control remains a vital question, as the short-term targets are only a proxy for the true endpoint; namely, survival. Nevertheless, the clinical outcome of the predefined target can be appropriately examined only with feedback control.

Manuscript received August 15, 2009. First published October 16, 2009; current version published December 01, 2009. This work was supported in part by the Japan Society for the Promotion of Science under Grant-in-Aid for Scientific Research (S) 18100006 and by the Ministry of Health Labour and Welfare of Japan under Health and Labour Sciences Research Grants H19-nano-ippan-009 and H20-katsudo-shitei-007.

M. Sugimachi is with the Department of Cardiovascular Dynamics, Advanced Medical Engineering Center, National Cardiovascular Center Research Institute, 5658565 Suita, Japan (e-mail: su91mach@ri.ncvc.go.jp).

K. Sunagawa is with the Department of Cardiovascular Medicine, Graduate School of Medical Sciences, Kyushu University, 8128582 Fukuoka, Japan (e-mail: sunagawa@cardiol.med.kyushu-u.ac.jp).

Digital Object Identifier 10.1109/RBME.2009.2034623